

Evaporation of Drops Containing Silica Nanoparticles of Varying Hydrophobicities: Exploiting Particle–Particle Interactions for Additive-Free Tunable Deposit Morphology

Manos Anyfantakis,^{*,†,‡} Damien Baigl,^{*,†,‡,§} and Bernard P. Binks^{*,§}

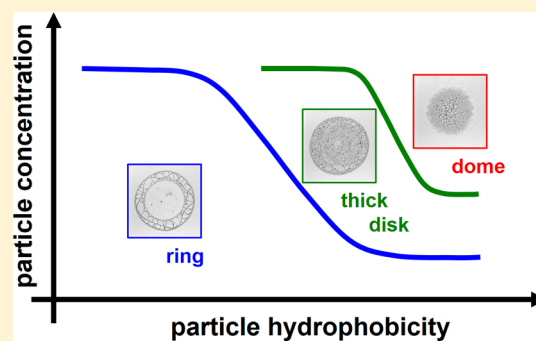
[†]École Normale Supérieure, PSL Research University, UPMC Univ Paris 06, CNRS, Department of Chemistry, PASTEUR, 24 rue Lhomond, 75005 Paris, France

[‡]Sorbonne Universités, UPMC Univ Paris 06, ENS, CNRS, PASTEUR, 75005 Paris, France

[§]School of Mathematics and Physical Sciences, University of Hull, Hull HU6 7RX, U.K.

Supporting Information

ABSTRACT: We describe the systematic and quantitative investigation of a large number of patterns that emerge after the evaporation of aqueous drops containing fumed silica nanoparticles (NPs) of varying wettabilities for an extended particle concentration range. We show that for a chosen system, the dry pattern morphology is mainly determined by particle–particle interactions (Coulomb repulsion and hydrophobic attraction) in the bulk. These depend on both particle hydrophobicity and particle concentration within the drop. For high and intermediate particle concentrations, interparticle hydrophobic attraction is the dominant factor defining the deposit morphology. With increasing particle hydrophobicity, patterns ranging from rings to domes are observed, arising from the time needed for the drop to gel compared with the total evaporation time. On the contrary, drops of dilute suspensions maintain a finite viscosity during most of the drop lifetime, resulting in dry patterns that are predominantly rings for all particle hydrophobicities. In all investigated systems, the NP concentration corresponded to a large excess of NPs in the bulk compared with the maximal amount that could be adsorbed at available interfaces, making particle–interface interactions such as adsorption of hydrophobic NPs at the air–water interface a negligible contribution over bulk particle–particle interactions. This work emphasizes the advantage of particle surface chemistry in tuning both particle–particle interactions and particle deposition onto solid substrates in a robust manner, without the need for any additive such as a surfactant.



I. INTRODUCTION

Control of the deposit pattern formed after the evaporation of a particle-laden sessile drop is important for numerous industrial applications, especially for inkjet printing, for coating substrates,¹ and for fabricating functional materials and devices.² Moreover, the pattern morphology plays a central role in various biotechnological applications such as DNA microarrays³ and has been recently recognized as a tool for particle patterning,⁴ for forensic investigations,⁵ and for cost-effective and robust diagnostic tools.^{6,7} Consequently, scientific efforts have focused in controlling the morphology of the patterns left behind following the evaporation of colloidal suspension drops.^{8,9} Perhaps, the most common obstacle that has to be circumvented is the “coffee ring effect” (CRE). The enhanced evaporation rate at the contact line of a pinned drop that dries on a solid substrate drives the solvent motion from the bulk to the drop edge. This capillary flow is capable of carrying dispersed particles or any other dissolved substance to the drop periphery, resulting in the familiar ring-shaped stains after complete evaporation.¹⁰

Whereas the CRE itself can be constructively used for functional colloidal patterning,¹¹ the most common requirement for uniform deposits led researchers to the in-depth exploration of the complex phenomena behind the CRE,¹² the understanding of which is a prerequisite for the successful manipulation of the stain morphology. Along these lines, following the seminal work of Deegan and co-workers,¹⁰ a large number of experimental and theoretical studies have been conducted to improve our understanding on particle deposition and pattern formation from drying suspension drops.^{12–14} A plethora of parameters, including the drying conditions (such as the substrate temperature,¹⁵ the relative humidity,¹⁶ and the chemical composition of the phase surrounding the droplet¹⁷), the properties of the solid substrate (including its wettability¹⁸ or surface charge¹⁹), and the properties of the dispersed particles,²⁰ have been shown to drastically affect the morphology of the deposited patterns. The practically

Received: March 9, 2017

Revised: April 26, 2017

Published: April 27, 2017

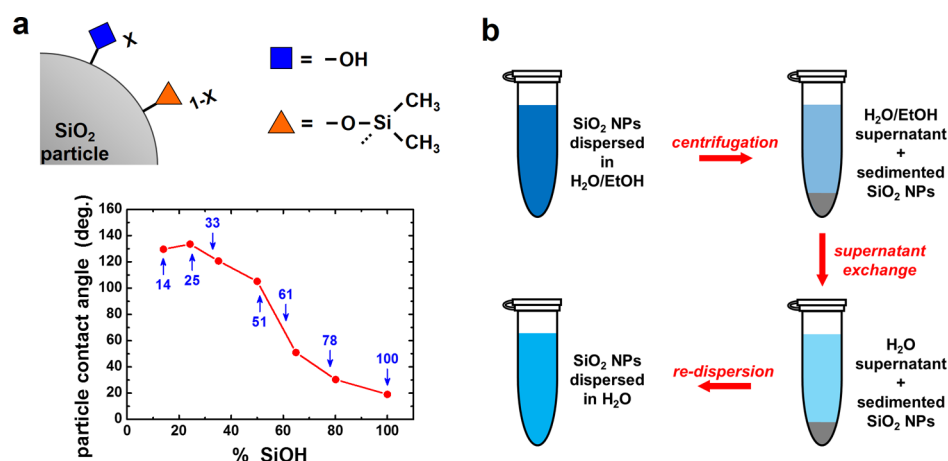


Figure 1. Preparation of concentrated aqueous suspensions of silica NPs of varying hydrophobicities. (a) Top: The molar fraction (X) of SiOH groups on particle surfaces was varied from 100 to 14% by means of controlled silanization with dichlorodimethylsilane. Bottom: Air–water particle contact angle as a function of X according to Kostakis et al. (red points).³⁶ The X values of the particles used in this study are indicated by blue arrows. (b) Route followed for the preparation of concentrated stock suspensions (20 mg/mL) of NPs possessing 51–14% SiOH. These hydrophobic batches were first dispersed in ethanol/water mixtures, and ethanol was subsequently removed by centrifugation followed by supernatant exchange, to finally obtain purely aqueous suspensions.

unlimited combinations of the above-mentioned sets of parameters make drawing of general conclusions difficult.

Regarding particle properties, the influence of size,^{21,22} shape,^{23,24} and surface charge^{24,25} has been explored in detail. On the contrary, the effect of particle hydrophobicity on the stain morphology resulting from evaporating drops has been largely neglected. Shao et al.²⁶ studied the deposition behavior of sessile drops containing micron-sized colloids that were left to dry on bare and silanized glass slides. Two particles of different hydrophobicities were used (more hydrophobic copolymer particles and more hydrophilic silica particles), whereas all other parameters (particle size, volume fraction, and drop volume) were kept comparable. After drying, concentric rings were formed for the dispersions containing copolymer particles, whereas drops with silica particles formed spokes that were perpendicular to the contact line. Two models were proposed to explain the observed patterns: the first one linked the flow patterns and the drag force acting on the particles and the second one involved the capillary interactions between the particles. Both models confirmed that the observed behavior could be attributed to the particle contact angle at the air–water interface.

Noncovalent modification of particle surface chemistry was shown to have a strong impact on the deposit morphology from evaporating colloidal suspension drops.^{27,28} In particular, the CRE could be totally suppressed using oppositely charged mixtures of surfactants and polystyrene latex particles. In a specific narrow window of surfactant concentrations, well below the critical micelle concentration, electrostatic surfactant adsorption on the particle surface resulted in particle neutralization. At the same time, particle wettability by water was decreased because the hydrophobic tails of the surfactant molecules interacted with water. The combination of these effects led to an enhanced particle affinity for the liquid–gas (LG) interface. Particle adsorption and subsequent aggregation at the free interface resulted in the formation of a jammed interfacial skin, preventing the participating particles from being transported to the drop edge by the radial outward flow. The deposition of the skin on the substrate at the end of the evaporation process led to a uniform pattern displaying a

disklike morphology.²⁸ With photosensitive surfactants,²⁹ this process could be controlled using light.²⁷

The influence of particle adsorption at the free interface on the CRE was partially discussed in a recent paper by Dugyala and Basavaraj.²⁴ Adsorption of hematite ellipsoids at the LG interface was favored at intermediate pH = 6.5, where the ellipsoids were weakly charged. Drying drops from such suspensions yielded rings when a hydrophobic glass substrate was used, whereas homogeneous patterns were obtained on hydrophilic glass. Although the authors concluded that the particle–substrate interactions were dominant,²⁴ the expected decrease in particle hydrophilicity and thus the possible increased particle affinity for the LG interface cannot be completely excluded as a contributing factor affecting the dry pattern morphology.

The ability of colloidal particles to adsorb at fluid–fluid interfaces and therefore to stabilize dispersed systems has been a subject of intense research activity, especially during the past 2 decades. Very stable emulsions and foams could be produced using colloidal particles alone as the stabilizer for the liquid–liquid and LG interfaces, respectively, without the need to use surfactants.^{30,31} A key parameter that influences particle adsorption at the interface is the contact angle θ that the particles make with the fluid–fluid interface (conventionally measured through the water phase). If θ lies within the correct range, the adsorption energy per particle can reach several thousands of $k_B T$ (k_B is the Boltzmann constant and T is the temperature), making the particles irreversibly attached to the interface.³⁰ In particular, chemically modified silica nanoparticles (NPs) of intermediate hydrophobicity were shown to form highly stable air bubbles dispersed in water³² and very stable foams in which aggregates were attached at the air–water interface.³³ It is important to note that aqueous foams share some analogies with sessile water drops because of the presence of a curved LG interface.

Bearing the above in mind and given our previous knowledge on the suppression of the CRE because of the surfactant-induced particle hydrophobization in oppositely charged mixtures of these two components,²⁸ we hypothesized that the inherent (i.e., chemically induced) hydrophobicity of silica

NPs similar to the ones used earlier^{32,33} should have a direct impact on the morphology of deposits left from the drying drops. To test this hypothesis and address the effect of particle hydrophobicity, we used a well-characterized system consisting of silica NPs dispersed in water. Their hydrophobicity was finely tuned by varying the extent of the surface silanol (SiOH) groups, which reacted with a silanizing agent. Apart from the well-controlled particle surface chemistry, an additional advantage of using this model system is that the absence of surfactants excludes solute Marangoni flows³⁴ (arising from surface tension gradients along the LG interface of the drop) and surfactant-mediated particle–interface interactions,^{9,28} which are able to influence the morphology of the dry patterns. We systematically analyze the patterns formed from the evaporation of sessile drops containing these modified silica NPs as a function of particle hydrophobicity and concentration. Morphological features were characterized using microscopy and were precisely quantified using profilometry. We uncovered, in particular, the coupling between particle surface chemistry, bulk interactions, and distribution of deposited particles upon drop evaporation.

II. EXPERIMENTAL SECTION

II.1. Materials. The fumed silica NPs used in this study were provided by Wacker Chemie (Germany) and were used as received. The diameter of individual NPs is 20–30 nm, with NP aggregates of sizes on the order of a few hundred nanometers being common. The NP surface was rendered hydrophobic by the reaction of the silanol groups with dichlorodimethylsilane.³⁵ NPs with a relative SiOH content ranging from 100 to 14% were used in this study (Figure 1a, top). The relative SiOH content was determined by titration with a base. According to Kostakis et al.,³⁶ the particle contact angle at the air–water interface was expected to significantly and continuously increase when the SiOH fraction decreased from 100 to 14% (Figure 1a, bottom), showing that our particles spanned a whole range of hydrophobicity, from very low (100% SiOH) to very high (14% SiOH).

Ultrapure water (resistivity 18.2 M Ω cm) was used for all experiments. Ethanol (Sigma-Aldrich) was used as a cosolvent for the preparation of suspensions containing the more hydrophobic particles (see below).

II.2. Preparation of NP Suspensions. For the preparation of the stock suspension (20 mg/mL), the required mass of NP powder was added to a glass vial, followed by the addition of the solvent. The three more hydrophilic batches, containing 100–61% SiOH groups, were directly dispersed in water. All other batches were initially dispersed in ethanol/water mixtures of different compositions as follows: The 51% SiOH batch was dispersed in a 5 wt % ethanol/water mixture, batches with 33 and 25% SiOH were dispersed in 10 wt % mixtures, and the most hydrophobic batch (14% SiOH) was dispersed in a 20 wt % ethanol/water mixture. The samples underwent vortexing and sonication cycles of varying durations until appearing macroscopically homogeneous. For the more hydrophilic NPs (100–61% SiOH), short times were sufficient for homogenization (min to h). Contrarily, a large number of cycles (over periods from several days to weeks) were required for all other NP suspensions because of their hydrophobicity and a strong tendency to foam. In particular, batches containing 33 and 25% SiOH tended to form very stable foams, in agreement with previous reports.^{30,31}

Following homogenization, a purification procedure was followed to exchange the ethanol content with water for the suspensions containing NPs with 51–14% SiOH groups (Figure 1b). The homogeneous dispersions (1.8 mL) were transferred to 2 mL Eppendorf tubes. Initially, they were typically centrifuged at 15 000 rpm for 30 min leading to NP sedimentation. Next, a large volume of the supernatant liquid (typically 1.0–1.4 mL) was exchanged with an equal volume of ultrapure water using a micropipette (Eppendorf).

The new suspension was homogenized again by applying the appropriate number of vortexing/sonication cycles. This procedure was repeated five times for each stock suspension to minimize the remaining amount of ethanol in the dispersions of silica NPs. Suspensions with lower solid content (10–0.5 mg/mL) were further prepared by diluting the stock suspensions with ultrapure water. The final particle concentrations explored in this study thus ranged from 0.5 to 20 mg/mL, which corresponded to volume fractions ranging from 0.23×10^{-3} to 9.1×10^{-3} , respectively.

II.3. Particle Aggregation State. According to Zang et al.,³⁷ fumed silica particles are clusters of irreversibly bound primary silica particles, the latter being quasi-spherical of approximately 20 nm diameter. Stocco et al.³⁸ characterized freshly sonicated aqueous dispersions of particles containing 34% SiOH. They found that the clusters making up the dispersions displayed a hydrodynamic radius $R_h = 85$ nm and a radius of gyration $R_g = 71$ nm. The ratio $R_h/R_g = 1.2$, being close to $(5/3)^{0.5}$, indicated that these aggregates had approximately spherical shapes. Furthermore, they were fairly monodisperse, displaying a polydispersity index of about 0.2. Finally, according to Horozov et al.,³⁹ such very stable aggregates were loosely bound together in larger agglomerates, which could be easily destroyed by sonication. We can thus assume that in our dispersions we had (i) mostly stable aggregates of hydrodynamic radius $R_h \approx 85$ nm accompanied by primary particles ($R_h \approx 10$ nm) and (ii) a few loosely bound large agglomerates (i.e., larger than the stable aggregates) because most of them are expected to be destroyed by the sonication procedure.

II.4. Drop Deposition and Drying. Before each drop evaporation experiment, the suspensions were sonicated for 30 min and were shaken gently by hand to avoid foaming. A drop (0.8 μ L) was then deposited on the substrate using a micropipette, and it was covered with a box to avoid air currents. All drying experiments were performed at a temperature and a relative humidity range of 22.0 ± 0.5 °C and $40.0 \pm 0.5\%$, respectively, unless stated otherwise. The utilized substrates were glass coverslips (Menzel-Gläser) and were used as received. There are two reasons for not cleaning the coverslips. First, we have noticed in earlier experiments that rinsing the coverslips with organic solvents and/or sweeping them with solvent-wet tissues led to irreproducible results regarding drop contact line pinning and dry deposit morphology. Second, more drastic cleaning procedures (e.g., plasma or piranha cleaning) typically lead to contact angles close to zero. We measured the water contact angle in air, and we found that it did not vary significantly from one substrate to another ($56.8 \pm 4.7^\circ$, Figure S1).

II.5. Imaging of the Deposits. Transmission bright field images of the deposited patterns and videos of the evaporating processes were captured using an inverted optical microscope (Zeiss Axio Observer) equipped with an EMCCD camera (PhotonMax 512, Princeton Instruments). Köhler illumination conditions were set before the experiments. All bright field images were acquired under similar illumination conditions and acquisition settings; they are displayed without any postprocessing. The dark field images are shown in Figures S2 and S3, to assist the observation of patterns, which had very low optical contrast in the bright field images. Each drying experiment was performed in triplicate and led to highly reproducible morphologies for most deposits (Figures S4–S6), except in rare cases when depinning occurred.

II.6. Surface Profilometry. Height profile measurements of the dry patterns were performed using a stylus profilometer (Dektak XT, Bruker). The measurements were recorded using a stylus setting of 1.5 mg and a lateral resolution of 0.28 μ m/pt. Typically, five individual scans were performed over an area 40 μ m wide and 2.5 mm long, separated by a distance of 10 μ m, along the center of the deposited pattern (Figure S7a). Under these conditions, individual scans provided similar profiles (Figure S7b,c) and were averaged to be displayed in Figures 2 and 5.

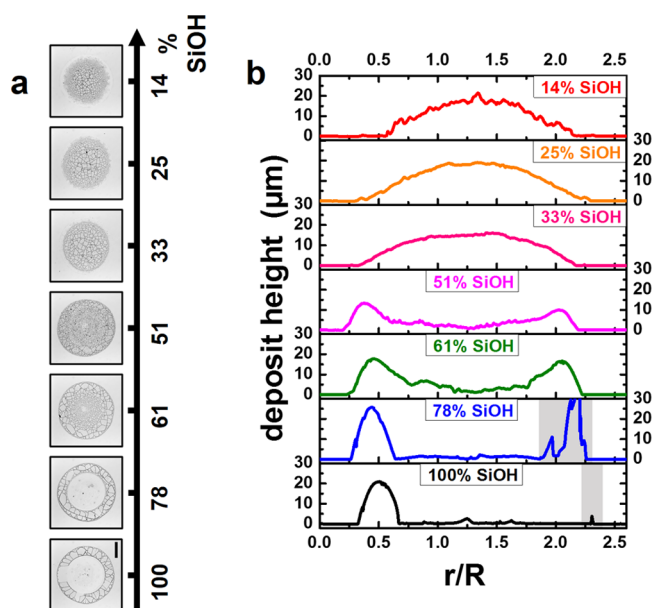


Figure 2. Morphologies of the patterns formed after the evaporation of sessile drops ($0.8 \mu\text{L}$) of highly concentrated stock suspensions (20 mg/mL) deposited on glass coverslips. Suspensions contained silica NPs possessing varying amounts of SiOH surface groups (100–14%) dispersed in water. (a) Transmission bright field microscope images of the dry deposits. The scale bar is $500 \mu\text{m}$. (b) Corresponding height profiles measured using a stylus profilometer. R is the deposit radius, and r is the radial dimension. Gray-shaded areas indicate parts of the profiles that were disturbed due to dragging of broken parts of the ring structure by the profilometer tip (see main text).

III. RESULTS AND DISCUSSION

III.1. Influence of Particle Hydrophobicity on the Dry Pattern Morphology for High Solid Content (20 mg/mL) Drops.

We first investigated deposits obtained from the highly concentrated suspensions (20 mg/mL). We placed $0.8 \mu\text{L}$ of the drops on glass coverslips, and we observed the patterns after complete drying. Figure 2 shows (a) the transmission bright field images and (b) the corresponding height profiles for the patterns arising from suspensions containing NPs of different SiOH contents. Overall, we observed a general trend of particle distribution on the substrate as a function of particle hydrophobicity. Hydrophilic particles were preferentially

deposited at the drop periphery, whereas increasing hydrophobicity led to an increasing number of particles in its center.

First, the drying drops of a dispersion containing the most hydrophilic NPs (100 and 78% SiOH) led to the formation of a typical ring-shaped deposit. The almost complete absence of NPs deposited in the interior of the dry pattern was confirmed by the profilometry data, showing an almost zero deposit height. This can be explained by the evaporation-driven convective outward flow¹⁰ that transported almost all NPs to the edge of the sessile drop, concentrating them at and near the pinned contact line. The thick ring deposit contained several cracks that were created during the very last stage of drying. Cracking in evaporating films containing particles is a common phenomenon^{40–42} observed in a plethora of diverse colloidal dispersions^{43–45} and is attributed to the development of large capillary stresses as the solvent dries.⁴⁶ Delamination spontaneously occurred in some cases, leading to empty areas within the ring deposit (Figure 2a). The ring deposit was found to be brittle. For instance, during profilometry experiments, the stylus tip frequently induced the breaking of the deposit and in some cases dragged the broken pieces during the measurement. In those specific cases (gray-shaded regions in height profiles), profilometry data did not reflect the actual pattern morphology before scanning. For this reason, microscope images were acquired before profilometry experiments.

The situation started to significantly change for intermediate hydrophobicities (61 and 51% SiOH). The microscope image showed a deposit consisting of two distinguishable regions (Figure 2a). A ring region encircled an interior homogeneous region, with different crack morphologies characterizing each region. The corresponding height profile (Figure 2b) showed a broader and slightly lower ring region compared with that obtained with the more hydrophilic particles (100 and 78% SiOH). The interior of the stain was covered by an increased number of deposited NPs, as indicated by the corresponding height ($\sim 5 \mu\text{m}$), showing a redistribution of the particles from the ring to the interior part. This effect was even more pronounced for the 51% SiOH NP system. In that case, an overall homogeneous deposit was observed using microscopy, with the ring and the interior phase being hardly distinguishable. The profilometry data indicated a rather homogenous height profile all along the deposit diameter.

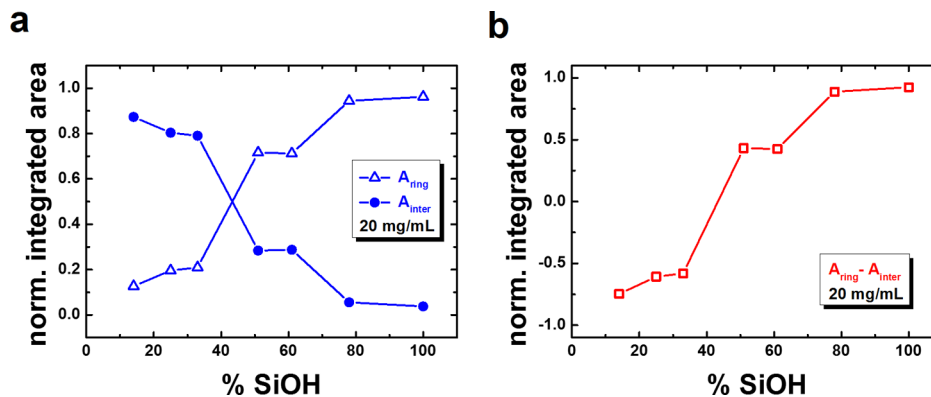


Figure 3. Quantification of the dry pattern evolution as a function of NP hydrophobicity for suspensions of 20 mg/mL . (a) Evolution of the normalized integrated area of the ring, A_{ring} (triangles), and the interior part of the deposit, A_{inter} (circles), vs the fraction of SiOH groups on silica NP surfaces. Note that A_{ring} and A_{inter} correspond to the normalized number density per unit length of NPs deposited in the ring and in the interior area of the stain, respectively. (b) Evolution of the difference $A_{\text{ring}} - A_{\text{inter}}$ (squares) vs the fraction of SiOH groups on silica NP surfaces.

A third type of behavior was observed when the most hydrophobic NPs (33 to 14% SiOH) were used. For the 33% SiOH NP system, a homogeneous pattern of smaller diameter (compared with the ones described above for more hydrophilic NPs) was observed in the microscope image (Figure 2a). The smaller deposit size was attributed to partial contact line depinning, contrary to the 100% SiOH–61% SiOH NP dispersions where the contact line remained firmly pinned during the whole drying process. The three-dimensional structure of this homogeneous deposit was, however, different from the one corresponding to the 51% SiOH system. The height profile (Figure 2b) was dome-shaped rather than being flat, that is, the particle number density continuously increased on approaching the drop center. Similar dome-shaped stains were also observed for the two most hydrophobic batches (25 and 14% SiOH content), with the most hydrophobic one being the smallest in diameter and the largest in height. It is worth noting that for all of these dome patterns, a tiny ring (height ≈ 0.5 – $1.5 \mu\text{m}$) outside the dome area could be observed, indicating the initial position of the contact line after drop deposition, which depinned later on.

III.2. Quantification of Pattern Evolution for High Solid Content (20 mg/mL) Drops. In an effort to quantify the observed deposition evolution as a function of particle wettability, we systematically analyzed the height profile data deduced from the patterns shown in Figure 2a. Figure 3 shows the normalized integrated areas occupied by the ring, A_{ring} , and the interior region, A_{inter} , for the stains obtained from the 20 mg/mL suspensions. These were calculated as

$$A_{\text{ring}} = \frac{a_{\text{ring}} / l_{\text{ring}}}{\frac{a_{\text{ring}}}{l_{\text{ring}}} + \frac{a_{\text{inter}}}{l_{\text{inter}}}} \quad \text{and} \quad A_{\text{inter}} = \frac{a_{\text{inter}} / l_{\text{inter}}}{\frac{a_{\text{ring}}}{l_{\text{ring}}} + \frac{a_{\text{inter}}}{l_{\text{inter}}}}. \quad l_{\text{ring}} \text{ is the sum of the lengths covered by the left and the right ring regions and } l_{\text{inter}} \text{ is the length occupied by the interior part of the deposit. Analogously, } a_{\text{ring}} \text{ is the sum of the integrated areas under the height profile curve for the left and right ring deposits and } a_{\text{inter}} \text{ is the integrated area under the height curve corresponding to the interior deposit region. The physical meaning of } A_{\text{ring}} \text{ and } A_{\text{inter}} \text{ is that they correspond to the normalized number density per unit length for the particles populating the ring and the interior area of the stain, respectively. For a detailed description of the methodology followed, see Text S1 and Figure S8.}$$

the lengths covered by the left and the right ring regions and l_{inter} is the length occupied by the interior part of the deposit. Analogously, a_{ring} is the sum of the integrated areas under the height profile curve for the left and right ring deposits and a_{inter} is the integrated area under the height curve corresponding to the interior deposit region. The physical meaning of A_{ring} and A_{inter} is that they correspond to the normalized number density per unit length for the particles populating the ring and the interior area of the stain, respectively. For a detailed description of the methodology followed, see Text S1 and Figure S8.

A clear separation of the normalized integrated areas corresponding to the ring (A_{ring}) and the disk (A_{inter}) can be seen for the two most hydrophilic batches of 100 and 78% SiOH (Figure 3a). A_{ring} values approached 1, indicating that essentially all hydrophilic NPs were deposited near the contact line of the dispersion drop. The values of A_{ring} significantly decreased to 0.71 (and A_{inter} values significantly increased to 0.29) for the drops obtained after the drying of the 61 and 51% SiOH suspension drops. This decrease indicated the homogenization tendency with decreasing particle wettability. Compared with the two most hydrophilic batches, less particles were gathered at the ring area, whereas more particles occupied the interior of the formed deposit. Despite the partial homogenization, the pattern was still predominantly a ring because $A_{\text{ring}} > A_{\text{inter}}$. For the three more hydrophobic NPs, containing 33, 25, and 14% SiOH, the situation was reversed because $A_{\text{inter}} > A_{\text{ring}}$. This is in agreement with the dome morphology observed in the height profile (Figure 2b), with the maximum number of NPs being deposited at the center of the dry pattern. In addition, it could be observed that A_{inter} slightly increased with decreasing particle hydrophobicity, reaching a

value of 0.87 for the most hydrophobic batch (14% SiOH, Figure 3a).

In summary, three regimes of deposit morphologies were observed for the drying drops containing silica NPs at 20 mg/mL. This is shown in Figure 3b, where the difference $A_{\text{ring}} - A_{\text{inter}}$, indicative of the tendency of NPs to be preferably deposited at the drop edge ($A_{\text{ring}} - A_{\text{inter}} \rightarrow 1$), at the drop interior ($A_{\text{ring}} - A_{\text{inter}} \rightarrow -1$), or distributed evenly along the drop diameter ($-1 < A_{\text{ring}} - A_{\text{inter}} < 1$), is plotted as a function of particle hydrophobicity. The hydrophilic NPs predominantly formed ring-shaped deposits, whereas the hydrophobic NPs formed dome-shaped deposits; particles with intermediate hydrophobicity resulted in stains displaying a more homogeneous morphology with characteristics between ring- and dome-shaped patterns.

III.3. Influence of Particle Hydrophobicity on the Dry Pattern Morphology from Drops of More Dilute (1–10 mg/mL) Suspensions. We continued by examining the patterns formed after the drying of silica NP suspension drops with a lower solid content, exploring the range from 10 mg/mL down to 1 mg/mL. This lower limit was set by the fact that drops of more dilute suspensions (0.5 mg/mL) yielded irregular patterns because of contact line depinning in most of the cases (Figure S2). Our goal was to identify whether the strong influence of particle wettability on the evolution of the dry deposit morphology, seen for the concentrated (20 mg/mL) systems, was at work for more dilute dispersions.

Figure 4 shows the bright field microscope images of dried drops of dispersions containing NPs of different hydro-

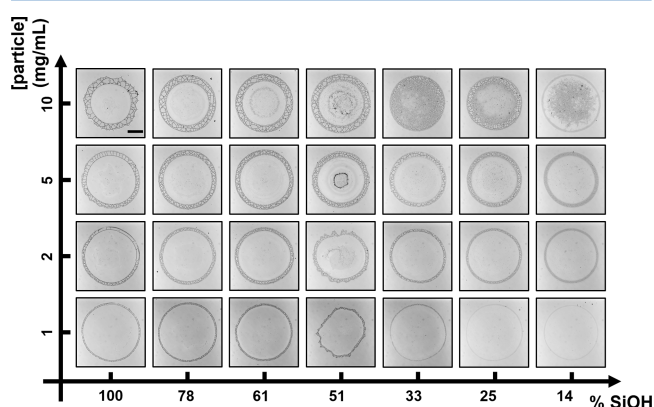


Figure 4. Transmission bright field microscope images of deposits obtained after the evaporation of sessile drops ($0.8 \mu\text{L}$) of silica NP suspensions deposited on glass coverslips. Suspensions containing NPs with varying contents of surface SiOH groups for an extended range of particle concentrations (1–10 mg/mL) were examined. The scale bar (see top left image) is $500 \mu\text{m}$.

phobicities at different particle concentrations. For clarity, the same patterns observed using dark field microscopy are shown in Figure S3. The height profiles corresponding to the depicted deposits are shown in Figure 5, whereas the normalized integrated areas, A_{ring} , A_{inter} , and their difference, as a function of % SiOH are shown in Figure S9.

A clear pattern evolution with increasing particle hydrophobicity (decreasing % SiOH) could be observed for the 10 mg/mL dispersions. Both drops of dispersions containing 100 and 78% SiOH led to the formation of typical ring patterns after drying (Figure 4, top row). The only qualitative difference between the two patterns was the crack density, which was

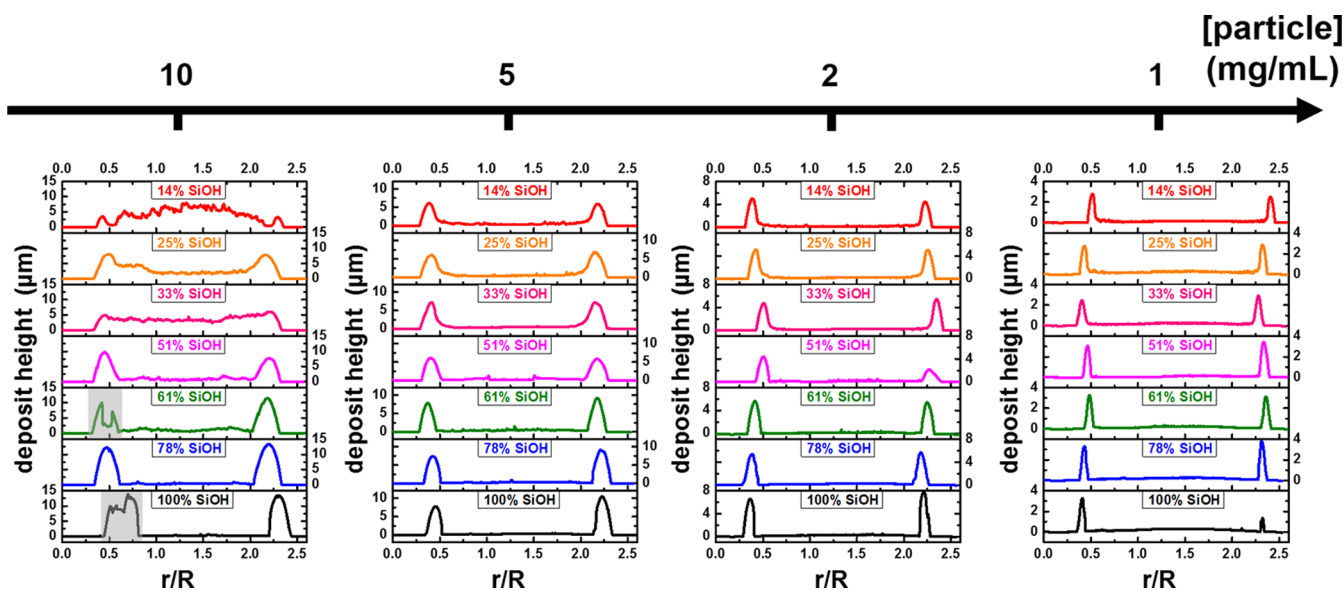


Figure 5. Height profiles of deposits obtained after the evaporation of sessile drops of silica NP suspensions deposited on glass coverslips. These profiles correspond to the patterns shown in Figure 4. Gray-shaded areas indicate parts of the profiles that were disturbed due to dragging of broken parts of the ring structure by the profilometer tip (see main text).

increased for the 78% system. The height profile data (Figure 5, left column and Figure S4) indicated that, for both hydrophilic batches, the vast majority of silica NPs were accumulated at the ring position ($A_{\text{ring}} = 0.96\text{--}0.97$), with the deposit interior containing almost no NPs ($A_{\text{interior}} = 0.03\text{--}0.04$). For drops containing 61 and 51% SiOH NPs, a tendency to pattern homogenization started to appear. The ring height progressively decreased with decreasing SiOH amount, from $\sim 15\ \mu\text{m}$ for the hydrophilic NPs (100 and 78% SiOH) to $\sim 10\ \mu\text{m}$ for the more hydrophobic systems (61 and 51% SiOH). At the same time, the fraction of particles occupying the deposit interior (resp. ring) started to increase (resp. decrease) for the more hydrophobic particles ($A_{\text{interior}} = 0.15\text{--}0.16$).

A dramatic change in the dry pattern morphology was observed by further increasing the hydrophobicity of the dispersed NPs (Figures 4 and S4). A completely homogeneous pattern was observed for the suspensions containing NPs with 33% SiOH (Figure 4, top row). The profilometry data (Figure 5, left column) revealed a thick disk-shaped morphology: the height of the deposit at its edge (i.e., at the position where a ring appeared for more hydrophilic NPs) equaled the height of the interior area, both assuming a value of about $5\ \mu\text{m}$ ($A_{\text{ring}} = 0.53$). A similar but slightly less homogeneous pattern was observed for the even more hydrophobic NPs having 25% SiOH content. In this case, two regions could be distinguished: an outer ring region containing a large density of cracks encircling a homogeneous interior region that was almost crack-free. The corresponding height profile supported such a picture, as an overall homogeneous pattern consisting of a broadened ring (height $\approx 8\ \mu\text{m}$) containing an inner area of decreased height of about $4\text{--}5\ \mu\text{m}$ was observed ($A_{\text{ring}} = 0.68$). Finally, when the most hydrophobic particles (14% SiOH content) were used, the obtained pattern was a dome encircled by a ring of very small ($< 5\ \mu\text{m}$) height, as evidenced by the microscope image and the corresponding height profile ($A_{\text{ring}} = 0.23$).

Interestingly, the evolution of the deposit morphology from the drying dispersions of lower particle concentrations (1–5 mg/mL) was found to be much less sensitive to particle

hydrophobicity. In general, we observed that all dry patterns were predominantly ring-shaped irrespective of particle hydrophobicity (Figures 4, S5, S6). However, the crack morphology and density in the rings changed significantly with varying particle wettability. This is in accordance with recent studies, which have demonstrated that the crack shape is strongly affected by the surface chemistry and hence by the interactions between the colloidal particles.⁴³ The height profile data and the extracted A_{ring} and A_{interior} values revealed two main trends. The ring height (Figure 5) decreased with a decrease in % SiOH on particle surfaces. At the same time, the integrated interior area A_{interior} seemed to slightly increase (Figure S9). These observations suggest that increasing the particle hydrophobicity tended to drive more particles into the deposit interior and thus marginally reduced the amount of NPs deposited at the ring position. This can be qualitatively seen for the 1 mg/mL drops of the two most hydrophobic NPs (25 and 14% SiOH; Figure 4, bottom row). In this case, the low ring height in combination with the (relatively) significant amount of NPs deposited in the stain interior caused small refractive index variations and thus a weak optical contrast between the ring and the interior areas. However, the profilometry data (Figure 5, right column) clearly showed that the pattern was still a ring, with the heights at the edge and the interior being ~ 3 and $< 1\ \mu\text{m}$, respectively ($A_{\text{ring}} = 0.88\text{--}0.92$).

Overall, we observed that particle hydrophobicity had a major influence on the dry pattern morphology emerging from evaporating drops for the two highest suspension concentrations examined (10 and 20 mg/mL). A ring \rightarrow thick disk \rightarrow dome deposit evolution was observed upon decreasing the number of SiOH groups on the NP surface. Conversely, for the more dilute suspensions (1–5 mg/mL), NPs were preferentially deposited at the ring position during drying, largely independent of the extent of NP hydrophobization.

III.4. Influence of Particle Concentration on the Dry Pattern Morphology. The influence of particle hydrophobicity on the morphological features of the dry deposit was clearly affected by the initial dispersion concentration (Figures 4 and 5). To investigate this on a more quantitative

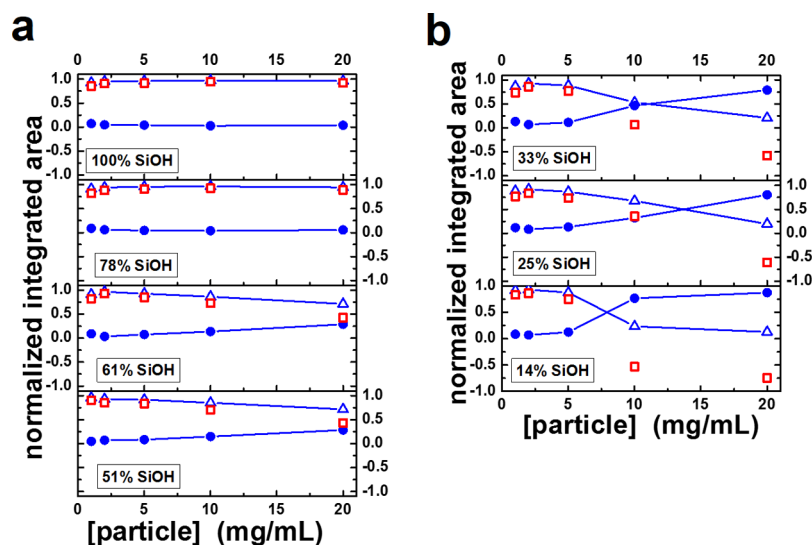


Figure 6. Quantification of the dry pattern evolution as a function of particle concentration for dispersions containing silica NPs of varying hydrophobicities. The evolutions of normalized ring area A_{ring} (triangles), interior area A_{inter} (circles), and their difference $A_{\text{ring}} - A_{\text{inter}}$ (squares) vs NP concentration are shown for 100–51% (a) and 33–14% (b) SiOH contents. These results were obtained by analyzing the height profiles shown in Figures 2 and 5.

basis, in Figure 6, we plot A_{ring} , A_{inter} , and their difference, $A_{\text{ring}} - A_{\text{inter}}$, as a function of particle concentration for all NP hydrophobicities.

For the two most hydrophilic batches containing 100 and 78% SiOH groups, $A_{\text{ring}} = 0.91\text{--}0.97$ (Figure 6a). This means that for the whole particle concentration range examined here (1–20 mg/mL), practically all NPs were accumulated in the ring area, whereas almost no particles were deposited in the stain interior. For the next two particle types of decreased wettability (61 and 51% SiOH), A_{ring} was always larger than A_{inter} ; however, their relative values were dependent on the initial particle concentration (Figure 6a). For suspensions containing 1–5 mg/mL silica NPs, $A_{\text{ring}} > 0.91$, indicating the accumulation of almost all NPs at the periphery of the dried droplet. For the patterns arising from the suspensions of intermediate concentration (10 mg/mL), $A_{\text{ring}} = 0.85$, showing that a small portion of NPs was deposited within the stain interior. For the concentrated suspensions (20 mg/mL), this partial homogenization tendency was even more evident, with A_{ring} being ~ 0.71 , indicating that a significant number of NPs (about 29%) were deposited within the area encircled by the ring.

For patterns arising from evaporating suspensions containing NPs with low content of silanol groups (33–14%), the evolution of A_{ring} and A_{inter} with NP concentration was different (Figure 6b). In the dilute regime (≤ 5 mg/mL), A_{ring} was 0.84–0.93, the signature of typical coffee ring patterns. On the contrary, A_{ring} strongly decreased for suspensions of increased NP concentration (10 mg/mL), assuming values of 0.53 and 0.68 for the 33 and 25% batches, respectively. More interestingly, A_{inter} (0.77) was larger than A_{ring} (0.23) for the suspension containing the most hydrophobic NPs with 14% SiOH content, in agreement with the observed dome-shaped morphology. For the concentrated NP regime of 20 mg/mL, A_{inter} was always larger than A_{ring} with the former values being in the range 0.79–0.87. This showed that only a small amount of NPs was deposited at the edge of the evaporating droplet.

On the basis of our experimental observations, we summarize the interplay of the effects of particle hydrophobicity and

concentration on the dry deposit morphology as follows. A general ring \rightarrow thick disk \rightarrow dome evolution with increasing NP hydrophobicity was documented. For the densest suspension drops, the full deposit spectrum could be observed. A decrease in the particle concentration led to a shift of this evolution to higher particle hydrophobicities, with the most dilute drops leading only to the initial part of the spectrum, i.e., ring patterns.

III.5. Influence of Particle Hydrophobicity and Concentration on Wetting Dynamics during Drying.

All experiments described before were devoted to the analysis of the final pattern characteristics. Because it is known that the dynamic evolution of the wetting behavior of a suspension drop during drying (contact angle and contact line pinning) can strongly affect the particle deposition,^{12,26,47} we explored how particle hydrophobicity and/or concentration influenced the wetting dynamics during evaporation. To this end, we systematically recorded the side profile of the evaporating drop and extracted the evolution of both contact angle and drop diameter as a function of time, for varying particle hydrophobicities and concentrations. First, we observed that, regardless of conditions, the drop slightly spread for about 1 min before the contact line reached a stable position, which was then maintained for nearly 80% of the total drying time (Figure S10). We first computed the initial contact angle, taken as the drop contact angle averaged in the time interval (70–80 s). This provided a measurement of the drop wettability in the early stage of stable pinning of the drop contact line. Figure S1 shows that the initial contact angle was slightly lower on average than the contact angle of a pure water drop on the same substrate but did not exhibit significant dependence on particle hydrophobicity or particle concentration. These results indicate that all drops started with a similar contact angle but led to different final patterns depending on the particle characteristics. The observed pattern evolution as a function of particle hydrophobicity and concentration cannot thus be related to variations in the contact angle. Such variations could have occurred, for instance, because of substrate-to-substrate variations or the presence of particles.

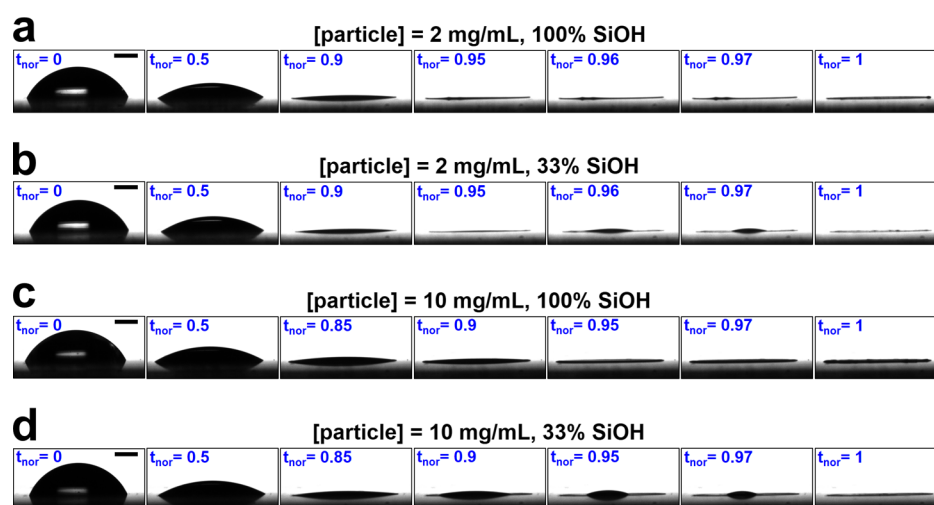


Figure 7. Evolution of the shape of a suspension drop ($1.5 \mu\text{L}$) as a function of the normalized time $t_{\text{nor}} = t/t_{\text{evap}}$ where t_{evap} is the total evaporation time of the drop for a particle concentration of (a,b) 2 mg/mL or (c,d) 10 mg/mL and a SiOH content of (a,c) 100% or (b,d) 33%. These experiments were conducted at a temperature and a relative humidity range of $22.2 \pm 0.4 \text{ }^\circ\text{C}$ and $23.5 \pm 0.5\%$, respectively. The full videos are available in *Movies S1, S2, S4, and S5*.

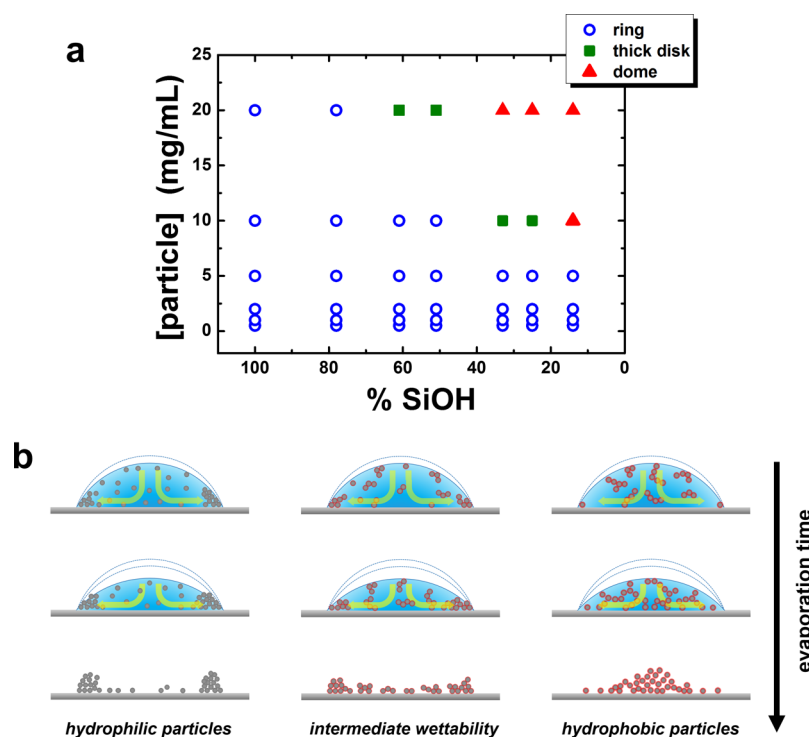


Figure 8. Summary of the dry pattern evolution as a function of the particle concentration and particle hydrophobicity, accompanied by our proposed explanation. (a) Qualitative pseudo-phase diagram summarizing the dry pattern morphology as a function of silica NP concentration and hydrophobicity. Note that, for the sake of simplicity, we categorize deposits as rings, thick disks, and domes. (b) Competition between NP transport to the drop edge caused by the evaporation-driven convective flow (yellow arrows) and NP immobilization due to suspension gelation defines the morphology of the dry deposit.

We then looked at the drop evolution dynamics during the whole evaporation process (Figure 7, *Movies S1–S6*). All drops had a similar behavior for more than 80% of the total evaporation time (t_{evap}), regardless of the particle hydrophobicity and the concentration (Figure S10). However, reproducible effects of the latter parameters could be detected in the late stage of evaporation. For hydrophilic and moderately hydrophobic particles (SiOH fraction $X \geq 51\%$), the contact line was maintained pinned, and the contact angle continuously

decreased until complete evaporation (Figure 7a,c). By contrast, for very hydrophobic particles, depinning was observed at a normalized time $t_{\text{nor}} = t/t_{\text{evap}}$ that slightly decreased with an increase in the particle concentration (Figure 7b,d). This was attributed to the contact line destabilization due to the presence of a significant amount of deposited hydrophobic particles, an effect that was amplified for higher particle concentrations. However, regardless of particle hydrophobicity, all samples at a low particle concentration ($\leq 2 \text{ mg/mL}$)

mL) led to similar ring patterns (Figure 5), showing that most of the material was deposited before contact line depinning started. In larger particle concentrations (≥ 10 mg/mL), contact line depinning was followed by a smoother drop receding at an approximately constant contact angle on a visibly thick deposit, which was in agreement with the presence of a rather homogenous deposit (Figure 5, SiOH fraction $X \leq 33\%$) underneath the receding drop. All of these results show that the wetting dynamics was only marginally affected by the presence of particles in the bulk of the drop suspension, with detectable effects only in the very late stages of evaporation, i.e., when most of particles had already been deposited. The particle concentration and the hydrophobicity thus seemed to direct the morphology of the deposited pattern, which could in turn affect the very late stage of drop drying.

III.6. Proposed Explanation. We here discuss the combined influence of (initial) particle concentration and particle hydrophobicity on the morphology of the deposits by gathering them in the form of a pseudo-phase diagram (Figure 8a); we further try to give a qualitative explanation for their formation (Figure 8b). For very hydrophilic particles, the deposits were always ring-shaped, irrespective of the NP concentration. As the wettability of the NPs decreased, the general pattern evolution was ring \rightarrow mixed ring/thick disk \rightarrow thick disk \rightarrow dome. However, the particle concentration was the parameter determining which parts of the above evolution could be observed. For low NP concentrations, the patterns were always rings, independent of particle hydrophobicity. For intermediate solid contents, a ring \rightarrow thick disk \rightarrow flattened dome tendency was realized. For the highly concentrated systems, the emergence of dome-shaped deposits was already observed at intermediate SiOH contents (which would lead to disks or rings for the more dilute suspensions).

Particle–particle interactions and therefore the phase behavior of colloidal suspensions critically depend on the surface chemistry of the constituent particles.⁴⁸ Consequently, in the systems investigated here, we expect that the interparticle potential was directly affected by the amount of SiOH groups on the NP surfaces. The interactions between nonmodified fumed silica NPs (100% SiOH) were predominantly electrostatic repulsions because of the negative NP surface charge when dispersed in ultrapure water. Decreasing the amount of SiOH groups by silanization led to weakened electrostatic repulsions and increasing attractive hydrophobic interactions. As a result, the colloidal stability progressively decreased with increasing NP hydrophobicity, as modified silica NPs tended to aggregate. This tendency was observed to be stronger with increasing particle concentration, as confirmed by the simple macroscopic observations of the suspension state. For the highly concentrated suspensions (20 mg/mL), the turbidity of the samples increased with decreasing SiOH content. This indicated that aggregation occurred in the systems, and the size of aggregates increased with increasing NP hydrophobicity. This is in agreement with the earlier work on similar particles, which reported that increasing the surface coverage of chemisorbed alkyl chains on fumed silica NPs led to their strong aggregation and therefore an increase in the suspension viscosity.⁴⁹ In our system, colloidal stability was also found to strongly depend on the NP concentration and hydrophobicity. For instance, the 20 mg/mL suspension of 14% SiOH NPs started to macroscopically phase separate (into a solvent-rich and a NP-rich phase) in only a few min after mixing. A similar phase behavior was observed for the 10 mg/mL suspensions of

the same NPs but at a longer timescale of a few tens of minutes; the more dilute suspensions were stable for at least several days.

The suspension phase behavior and its related rheological properties are two critical factors that affect the drying stage of a colloidal drop.⁵⁰ The type and magnitude of flows during drying can, in many cases, dictate the morphology of the final deposit.¹² In our system, the attractive interparticle potential, which is a function of NP wettability, directly influenced both the thermodynamic and rheological states of the suspension. The dominance of attractions (for hydrophobic NPs) led to the gelation of the system as the average NP volume fraction in the drop increased with the drying time. The critical time for the gelation transition to take place depended on the initial NP concentration. Indeed, it has been reported that hydrophobically modified fumed silica dispersed in polar solvents experienced strong attractive interactions because of the mismatch between the chemical nature of the NP surface and the continuous medium.⁵¹ Such hydrophobic attractions resulted in the formation of a volume-filling network of associated NPs and the gelation of the system.^{51,52}

The competition between the evaporation-driven radial outward flow and the gel transition is crucial in defining the dry deposit morphology in our systems. The radial flow of water molecules was omnipresent in our drying drops (due to contact line pinning), carrying along the dispersed particles as long as they are free to move. Gelation occurred either for high concentrations of NPs of intermediate hydrophobicity or for intermediate and high concentrations of NPs of high hydrophobicity. Hydrophilic NPs were always free to move and were carried at the edge of the drop because no gelation occurred at any solid content (Figure 8b, left). Suspensions containing hydrophobic NPs were kinetically arrested soon after drop deposition, and the resultant morphology after complete evaporation was a dome (Figure 8b, right). In fact, a dome morphology reflects the initially uniform NP distribution in a drop of a spherical cap shape, implying that the majority of suspended NPs were not significantly transported by the evaporation-driven flow during drop drying.⁵³ The critical time for the establishment of the network of particles (gel) depended on the initial particle content. For particles of intermediate wettability, both radial transport of particles and gelation were present, the former acting at short evaporation times and the latter at the later stages of drying (Figure 8b, middle). The amount of NPs dragged by the radial flow determined whether the dry stain would be more ringlike (with many NPs deposited in the interior), a flat thick disk, or more domelike.

The thick disk-shaped patterns observed in our study were similar to the so-called “pancake” stains observed in polystyrene NP suspensions containing Laponite particles.⁵³ In these systems, gelation occurred with increasing Laponite particle concentration during drop evaporation. Thus, by varying the initial Laponite concentration, Talbot et al. could modulate the time needed for the gel to appear and hence control the amount of radial flow. When gelation took place at intermediate times, the limited amount of radial motion led to the formation of homogeneous pancake deposits. On the other hand, very fast gelation led to the formation of domes because in that case, the particles became immobile soon after drop deposition and thus were not affected by the radial flow.⁵³ It is important to note that such morphologies are different from the thin “disk” morphology obtained when drying the drops containing oppositely charged surfactant–particle mixtures.^{27,28} In that

case, particle charge neutralization and hydrophobization caused by surfactant physisorption (within a narrow surfactant concentration window) increased the particle affinity for the LG interface. As a result, the surfactant-decorated particles were trapped at the free interface of the drop and formed a thin skin (typically a particle monolayer), the deposition of which led to homogeneous thin disks.

Adsorption of the hydrophobically modified silica NPs at the free interface of the drop is highly expected, especially for the NPs of intermediate wettability, as previously reported.^{33,39,54} We give here a simple estimate of the contribution of this two-dimensional effect to the deposit morphology in the dried drops. We assume that the radius of a primary fumed silica NP is $R_h = 10$ nm. The area of a typical dried deposit (radius 0.9 mm) is $A = 2.5 \times 10^{-6}$ m². To fill this area with a random close-packed monolayer (filling fraction 0.82)⁵⁵ consisting of N individual NPs, the following equation has to hold: $N\pi R_h^2/A = 0.82$. Here, we assumed for simplicity that the contact angle of the particles at the free interface is 90°. We thus need $N \approx 6.5 \times 10^9$ particles in a 0.8 μ L drop (typical volume used in our experiments), which corresponds to a particle concentration of about 0.07 mg/mL, taking the density of fumed silica as 2.2 g/cm³. The most dilute suspensions discussed here have a much higher concentration of 1 mg/mL. (Note that experiments with lower NP concentrations were carried out, but depinning of the contact line regularly occurred; see Figure S2.) This means that for all stains presented in this study, there are many more dispersed particles than the critical number needed to have a (single) NP monolayer that could lead to homogeneous thin-disk-shaped deposits.²⁸ Therefore, we can conclude that the bulk effect described above (gelation) will dominate, and the effect of NP adsorption at the interface, although probably present, will be insignificant in defining the stain morphology.

Finally, to evaluate the extent of sedimentation and its possible influence on the morphology of the deposits after drop evaporation, we calculated an adimensional Péclet number (Pe) that compared the transport by sedimentation to that by diffusion (Text S2). This calculation showed that (i) the primary particles were practically not affected by sedimentation ($Pe \ll 1$); (ii) for the stable aggregates (presumably the majority of objects in our drops), sedimentation and diffusion were almost equally important ($Pe \approx 1$); and (iii) for micrometer-sized agglomerates only (i.e., the small fraction that could not be destroyed by initial sonication or that would form during drop drying), sedimentation would dominate ($Pe \gg 1$). We can thus conclude that during drop evaporation, only very large agglomerates might settle on the substrate by sedimentation. On the contrary, the majority of the particles in the suspension drops, which are in the form of stable aggregates, should be subjected to both evaporation-induced flow and gravity. This is further evidence that the bulk effects described, and especially gelation, are crucial in counteracting the evaporation-driven flow that would otherwise transport the particles to the contact line.

IV. CONCLUSIONS

We hypothesized that the NP hydrophobicity in drying drops of colloidal suspensions should have a direct impact on the dry deposit morphology through the combined action of interfacial and bulk mechanisms. The former is related to the well-established tendency of partially hydrophobic NPs to adsorb and aggregate at the air–water interface. The latter is linked to the enhanced particle–particle attractions due to hydrophobic

interactions and its influence on the flow properties of the suspensions. To test this scenario, we used aqueous suspensions of fumed silica NPs of varying wettabilities. For hydrophilic NPs, the dry patterns always had a ring-shaped morphology for all particle concentrations investigated. For suspensions containing NPs of lower wettability, the particle concentration had a strong influence on the dry pattern morphology. As the hydrophobicity of the NPs increased, we observed a general ring \rightarrow mixed ring/thick disk \rightarrow thick disk \rightarrow dome deposit evolution. For dilute suspensions, ring-shaped deposits were obtained for the whole particle wettability range examined. For intermediate particle concentrations, a ring \rightarrow thick disk \rightarrow flattened dome evolution occurred. At high solid contents, a ring \rightarrow flattened dome \rightarrow steep dome progression was observed. The emergence of cracks during the very last stage of solvent evaporation was evident in all examined cases, regardless of the precise morphological characteristics of the dry patterns.

We showed that the wetting dynamics of the drop was only marginally affected by the presence of particles. The observed pattern evolution was thus mainly explained on the basis of particle–particle interactions in bulk and their direct influence on the state of the suspensions. Decreasing the amount of polar silanol groups on the particle surface strongly weakened the electrostatic interparticle repulsions. At the same time, this led to strong hydrophobic attractions arising from the increased mismatch between the physicochemical properties of the dispersed and continuous phases. These attractive interactions resulted in kinetically arrested gel states during drop drying. The critical time for gelation was dependent on the initial NP concentration and particle hydrophobicity.

The amount of particles transported to the drop contact line by the radial convective flow was crucial in defining the dry deposit morphology. This by itself depended on the critical time for the gel state to be established. For nongelling suspensions (infinite critical time and finite suspension viscosity), NPs were free to move and they could be effectively carried along with the radial flow to the drop edge, resulting in the ring stain. By contrast, associated particles forming the gel (finite critical time and diverging viscosity) were immobile and were not affected by the radial flow. In that case, dome-shaped deposits occurred, reflecting the particle concentration profile in a spherical cap-shaped sessile drop. Short critical gelling times led to patterns displaying a steep dome morphology. For suspensions characterized by longer critical times, both radial transport of particles and kinetic arrest of the system were present, the former acting at short evaporation times and the latter at the later stages of drying. The final patterns in such cases fell within the mixed ring/thick disk \rightarrow thick disk \rightarrow flattened dome group, depending on the amount of particles accumulated at the drop periphery. Because of the small particle size, the concentrations investigated here corresponded to a large excess of particles compared with the area of available interfaces (air–water and solid–water). As a consequence, the contribution of NP trapping at the air–water interface, although likely for nonhydrophilic colloids, or at the solid–water interface was a weak effect leaving the final pattern morphology largely unaffected.

■ ASSOCIATED CONTENT

Supporting Information

The Supporting Information is available free of charge on the ACS Publications website at DOI: 10.1021/acs.langmuir.7b00807.

Procedure for analyzing the morphology of deposits emerging after sessile drop evaporation, extent of sedimentation and its influence on the morphology of the deposits after drop evaporation, contact angle of drops of aqueous silica particle dispersions in air on glass coverslips as a function of the surface fraction of SiOH groups, morphologies of the patterns formed after the evaporation of sessile drops, transmission dark field and bright field microscope images of deposits obtained after the evaporation of sessile drops, schematic showing the relevant lengths (indicated with dashed lines) and integrated areas (in gray) used for the analysis of the deposit height profiles, quantification of dry pattern evolution as a function of particle hydrophobicity, and drop contact angle and drop base diameter as a function of time (PDF)

Side-view imaging of the evaporation of a 1.5 μL drop containing 2 mg/mL NPs with 100% SiOH content, which was deposited on a glass coverslip (MPG)

Side-view imaging of the evaporation of a 1.5 μL drop containing 2 mg/mL NPs with 33% SiOH content, which was deposited on a glass coverslip (MPG)

Side-view imaging of the evaporation of a 1.5 μL drop containing 2 mg/mL NPs with 14% SiOH content, which was deposited on a glass coverslip (MPG)

Side-view imaging of the evaporation of a 1.5 μL drop containing 10 mg/mL NPs with 100% SiOH content, which was deposited on a glass coverslip (MPG)

Side-view imaging of the evaporation of a 1.5 μL drop containing 10 mg/mL NPs with 33% SiOH content, which was deposited on a glass coverslip (MPG)

Side-view imaging of the evaporation of a 1.5 μL drop containing 10 mg/mL NPs with 14% SiOH content, which was deposited on a glass coverslip (MPG)

■ AUTHOR INFORMATION

Corresponding Authors

*E-mail: emmanouil.anyfantakis@ens.fr (M.A.).

*E-mail: damien.baigl@ens.fr (D.B.).

*E-mail: b.p.binks@hull.ac.uk (B.P.B.).

ORCID

Damien Baigl: 0000-0003-1772-3080

Bernard P. Binks: 0000-0003-3639-8041

Author Contributions

B.P.B. formulated the initial hypothesis that inherent particle hydrophobicity should strongly affect the particle deposition in drying drops. M.A., D.B., and B.P.B. designed the work. M.A. performed all experiments and data analysis and wrote the manuscript with input from D.B. and B.P.B.

Notes

The authors declare no competing financial interest.

■ ACKNOWLEDGMENTS

The authors would like to thank Dr. Tomo Kurimura for her assistance in the profilometry data analysis and Subramanyan N. Varanakkottu for helpful discussions. M.A. acknowledges

funding from the European Commission (FP7-PEOPLE-2013-IEF/Project 624806 “DIOPTRA”).

■ REFERENCES

- (1) Kim, D.; Jeong, S.; Park, B. K.; Moon, J. Direct Writing of Silver Conductive Patterns: Improvement of Film Morphology and Conductance by Controlling Solvent Compositions. *Appl. Phys. Lett.* **2006**, *89*, 264101.
- (2) Calvert, P. Inkjet Printing for Materials and Devices. *Chem. Mater.* **2001**, *13*, 3299–3305.
- (3) Blosssey, R.; Bosio, A. Contact Line Deposits on cDNA Microarrays: A “Twin-Spot Effect”. *Langmuir* **2002**, *18*, 2952–2954.
- (4) Zhang, Z.; Zhang, X.; Xin, Z.; Deng, M.; Wen, Y.; Song, Y. Controlled Inkjetting of a Conductive Pattern of Silver Nanoparticles Based on the Coffee-Ring Effect. *Adv. Mater.* **2013**, *25*, 6714–6718.
- (5) Zeid, W. B.; Brutin, D. Influence of Relative Humidity on Spreading, Pattern Formation and Adhesion of a Drying Drop of Whole Blood. *Colloids Surf., A* **2013**, *430*, 1–7.
- (6) Li, Y.; Zhao, Z.; Lam, M. L.; Liu, W.; Yeung, P. P.; Chieng, C.-C.; Chen, T.-H. Hybridization-Induced Suppression of Coffee Ring Effect for Nucleic Acid Detection. *Sens. Actuators, B* **2015**, *206*, 56–64.
- (7) Devineau, S.; Anyfantakis, M.; Marichal, L.; Kiger, L.; Morel, M.; Rudiuk, S.; Baigl, D. Protein Adsorption and Reorganization on Nanoparticles Probed by the Coffee-Ring Effect: Application to Single Point Mutation Detection. *J. Am. Chem. Soc.* **2016**, *138*, 11623–11632.
- (8) Sun, J.; Bao, B.; He, M.; Zhou, H.; Song, Y. Recent Advances in Controlling the Depositing Morphologies of Inkjet Droplets. *ACS Appl. Mater. Interfaces* **2015**, *7*, 28086–28099.
- (9) Anyfantakis, M.; Baigl, D. Manipulating the Coffee-Ring Effect: Interactions at Work. *ChemPhysChem* **2015**, *16*, 2726–2734.
- (10) Deegan, R. D.; Bakajin, O.; Dupont, T. F.; Huber, G.; Nagel, S. R.; Witten, T. A. Capillary Flow as the Cause of Ring Stains from Dried Liquid Drops. *Nature* **1997**, *389*, 827–829.
- (11) Layani, M.; Gruchko, M.; Milo, O.; Balberg, I.; Azulay, D.; Magdassi, S. Transparent Conductive Coatings by Printing Coffee Ring Arrays Obtained at Room Temperature. *ACS Nano* **2009**, *3*, 3537–3542.
- (12) Larson, R. G. Transport and Deposition Patterns in Drying Sessile Droplets. *AIChE J.* **2014**, *60*, 1538–1571.
- (13) Sefiane, K. Patterns from Drying Drops. *Adv. Colloid Interface Sci.* **2014**, *206*, 372–381.
- (14) Zhong, X.; Crivoi, A.; Duan, F. Sessile Nanofluid Droplet Drying. *Adv. Colloid Interface Sci.* **2015**, *217*, 13–30.
- (15) Parsa, M.; Harmand, S.; Sefiane, K.; Bigerelle, M.; Deltombe, R. Effect of Substrate Temperature on Pattern Formation of Nanoparticles from Volatile Drops. *Langmuir* **2015**, *31*, 3354–3367.
- (16) Chhasatia, V. H.; Joshi, A. S.; Sun, Y. Effect of Relative Humidity on Contact Angle and Particle Deposition Morphology of an Evaporating Colloidal Drop. *Appl. Phys. Lett.* **2010**, *97*, 231909.
- (17) Majumder, M.; Rendall, C. S.; Eukel, J. A.; Wang, J. Y. L.; Behabtu, N.; Pint, C. L.; Liu, T.-Y.; Orbaek, A. W.; Mirri, F.; Nam, J.; et al. Overcoming the “Coffee-Stain” Effect by Compositional Marangoni-Flow-Assisted Drop-Drying. *J. Phys. Chem. B* **2012**, *116*, 6536–6542.
- (18) Zhang, L.; Nguyen, Y.; Chen, W. “Coffee Ring” Formation Dynamics on Molecularly Smooth Substrates with Varying Receding Contact Angles. *Colloids Surf., A* **2014**, *449*, 42–50.
- (19) Yan, Q.; Gao, L.; Sharma, V.; Chiang, Y.-M.; Wong, C. C. Particle and Substrate Charge Effects on Colloidal Self-Assembly in a Sessile Drop. *Langmuir* **2008**, *24*, 11518–11522.
- (20) Crivoi, A.; Zhong, X.; Duan, F. Crossover from the Coffee-Ring Effect to the Uniform Deposit Caused by Irreversible Cluster-Cluster Aggregation. *Phys. Rev. E: Stat., Nonlinear, Soft Matter Phys.* **2015**, *92*, 032302.
- (21) Shen, X.; Ho, C.-M.; Wong, T.-S. Minimal Size of Coffee Ring Structure. *J. Phys. Chem. B* **2010**, *114*, 5269–5274.
- (22) Monteux, C.; Lequeux, F. Packing and Sorting Colloids at the Contact Line of a Drying Drop. *Langmuir* **2011**, *27*, 2917–2922.

- (23) Yunker, P. J.; Still, T.; Lohr, M. A.; Yodh, A. G. Suppression of the Coffee-Ring Effect by Shape-Dependent Capillary Interactions. *Nature* **2011**, *476*, 308–311.
- (24) Dugyala, V. R.; Basavaraj, M. G. Control over Coffee-Ring Formation in Evaporating Liquid Drops Containing Ellipsoids. *Langmuir* **2014**, *30*, 8680–8686.
- (25) Bhardwaj, R.; Fang, X.; Somasundaran, P.; Attinger, D. Self-Assembly of Colloidal Particles from Evaporating Droplets: Role of DLVO Interactions and Proposition of a Phase Diagram. *Langmuir* **2010**, *26*, 7833–7842.
- (26) Shao, F. F.; Neild, A.; Ng, T. W. Hydrophobicity Effect in the Self Assembly of Particles in an Evaporating Droplet. *J. Appl. Phys.* **2010**, *108*, 034512.
- (27) Anyfantakis, M.; Baigl, D. Dynamic Photocontrol of the Coffee-Ring Effect with Optically Tunable Particle Stickiness. *Angew. Chem., Int. Ed.* **2014**, *53*, 14077–14081.
- (28) Anyfantakis, M.; Geng, Z.; Morel, M.; Rudiuk, S.; Baigl, D. Modulation of the Coffee-Ring Effect in Particle/Surfactant Mixtures: The Importance of Particle–Interface Interactions. *Langmuir* **2015**, *31*, 4113–4120.
- (29) Diguët, A.; Guillermic, R.-M.; Magome, N.; Saint-Jalmes, A.; Chen, Y.; Yoshikawa, K.; Baigl, D. Photomanipulation of a Droplet by the Chromocapillary Effect. *Angew. Chem., Int. Ed.* **2009**, *48*, 9281–9284.
- (30) Binks, B. P. Particles as Surfactants—Similarities and Differences. *Curr. Opin. Colloid Interface Sci.* **2002**, *7*, 21–41.
- (31) Horozov, T. S. Foams and Foam Films Stabilised by Solid Particles. *Curr. Opin. Colloid Interface Sci.* **2008**, *13*, 134–140.
- (32) Dickinson, E.; Ettelaie, R.; Kostakis, T.; Murray, B. S. Factors Controlling the Formation and Stability of Air Bubbles Stabilized by Partially Hydrophobic Silica Nanoparticles. *Langmuir* **2004**, *20*, 8517–8525.
- (33) Binks, B. P.; Horozov, T. S. Aqueous Foams Stabilized Solely by Silica Nanoparticles. *Angew. Chem., Int. Ed.* **2005**, *44*, 3722–3725.
- (34) Still, T.; Yunker, P. J.; Yodh, A. G. Surfactant-Induced Marangoni Eddies Alter the Coffee-Rings of Evaporating Colloidal Drops. *Langmuir* **2012**, *28*, 4984–4988.
- (35) Binks, B. P.; Lumsdon, S. O. Influence of Particle Wettability on the Type and Stability of Surfactant-Free Emulsions. *Langmuir* **2000**, *16*, 8622–8631.
- (36) Kostakis, T.; Ettelaie, R.; Murray, B. S. Effect of High Salt Concentrations on the Stabilization of Bubbles by Silica Particles. *Langmuir* **2006**, *22*, 1273–1280.
- (37) Zang, D.; Stocco, A.; Langevin, D.; Wei, B.; Binks, B. P. An Ellipsometry Study of Silica Nanoparticle Layers at the Water Surface. *Phys. Chem. Chem. Phys.* **2009**, *11*, 9522.
- (38) Stocco, A.; Drenckhan, W.; Rio, E.; Langevin, D.; Binks, B. P. Particle-Stabilised Foams: An Interfacial Study. *Soft Matter* **2009**, *5*, 2215.
- (39) Horozov, T. S.; Binks, B. P.; Aveyard, R.; Clint, J. H. Effect of Particle Hydrophobicity on the Formation and Collapse of Fumed Silica Particle Monolayers at the Oil–Water Interface. *Colloids Surf., A* **2006**, *282–283*, 377–386.
- (40) Pauchard, L.; Parisse, F.; Allain, C. Influence of Salt Content on Crack Patterns Formed through Colloidal Suspension Desiccation. *Phys. Rev. E: Stat. Phys., Plasmas, Fluids, Relat. Interdiscip. Top.* **1999**, *59*, 3737–3740.
- (41) Dufresne, E. R.; Corwin, E. I.; Greenblatt, N. A.; Ashmore, J.; Wang, D. Y.; Dinsmore, A. D.; Cheng, J. X.; Xie, X. S.; Hutchinson, J. W.; Weitz, D. A. Flow and Fracture in Drying Nanoparticle Suspensions. *Phys. Rev. Lett.* **2003**, *91*, 224501.
- (42) Lazarus, V.; Pauchard, L. From Craquelures to Spiral Crack Patterns: Influence of Layer Thickness on the Crack Patterns Induced by Desiccation. *Soft Matter* **2011**, *7*, 2552.
- (43) Carle, F.; Brutin, D. How Surface Functional Groups Influence Fracturation in Nanofluid Droplet Dry-Outs. *Langmuir* **2013**, *29*, 9962–9966.
- (44) Giorgiutti-Dauphiné, F.; Pauchard, L. Elapsed Time for Crack Formation during Drying. *Eur. Phys. J. E* **2014**, *37*, 39.
- (45) Sobac, B.; Brutin, D. Desiccation of a Sessile Drop of Blood: Cracks, Folds Formation and Delamination. *Colloids Surf., A* **2014**, *448*, 34–44.
- (46) Routh, A. F. Drying of Thin Colloidal Films. *Rep. Prog. Phys.* **2013**, *76*, 046603.
- (47) Nguyen, T. A. H.; Hampton, M. A.; Nguyen, A. V. Evaporation of Nanoparticle Droplets on Smooth Hydrophobic Surfaces: The Inner Coffee Ring Deposits. *J. Phys. Chem. C* **2013**, *117*, 4707–4716.
- (48) Hunter, R. J. *Foundations of Colloid Science*, 2nd ed.; Oxford University Press: Oxford, 2001.
- (49) Lee, G.; Rupperecht, H. Rheological Properties of Non-Modified and n-Alkyl Surface-Modified Colloidal Silica Sols. *J. Colloid Interface Sci.* **1985**, *105*, 257–266.
- (50) Haw, M. D.; Gillie, M.; Poon, W. C. K. Effects of Phase Behavior on the Drying of Colloidal Suspensions. *Langmuir* **2002**, *18*, 1626–1633.
- (51) Raghavan, S. R.; Hou, J.; Baker, G. L.; Khan, S. A. Colloidal Interactions between Particles with Tethered Nonpolar Chains Dispersed in Polar Media: Direct Correlation between Dynamic Rheology and Interaction Parameters. *Langmuir* **2000**, *16*, 1066–1077.
- (52) Barthel, H. Surface Interactions of Dimethylsiloxy Group-Modified Fumed Silica. *Colloids Surf., A* **1995**, *101*, 217–226.
- (53) Talbot, E. L.; Yang, L.; Berson, A.; Bain, C. D. Control of the Particle Distribution in Inkjet Printing through an Evaporation-Driven Sol–Gel Transition. *ACS Appl. Mater. Interfaces* **2014**, *6*, 9572–9583.
- (54) Binks, B. P.; Murakami, R. Phase Inversion of Particle-Stabilized Materials from Foams to Dry Water. *Nat. Mater.* **2006**, *5*, 865–869.
- (55) Berryman, J. G. Random Close Packing of Hard Spheres and Disks. *Phys. Rev. A* **1983**, *27*, 1053–1061.